

Numerical and experimental analysis of a wave energy converter in extreme waves

Ignacio P. Johannesen^{*1}, José M. Ahumada²,
Gonzalo Tampier², Laura Grüter³ and Cristian Cifuentes²

¹School of Engineering, Computing and Mathematics, University of Plymouth, Plymouth, Devon, UK

²Institute of Naval Architecture and Ocean Engineering, General Lagos 2086, Campus Miraflores,
Universidad Austral de Chile Valdivia, Chile

³Dynamics of Maritime Systems, Technical University of Berlin, Berlin, Germany

(Received March 20, 2023, Revised August 10, 2023, Accepted August 17, 2023)

Abstract. In the present paper, a numerical and experimental analysis for a wave energy converter under extreme environmental conditions is carried out. After the definition of design waves, including a 100-year return period stochastic sea state and a deterministic rogue wave condition, a numerical analysis using potential theory and a RANS equations solver are compared with experiments carried out at the Seakeeping Basin at the Technical University of Berlin. Results are discussed with special emphasis on the limits of potential theory methods for the evaluation of extreme wave conditions and the use of the presented methodology for early design stages.

Keywords: CFD simulation; experimental hydrodynamics; marine energy; WEC

1. Introduction

Today, wave energy converters are still considered in a pre-commercial stage of development, facing important challenges in areas such as affordability, survivability, maintainability, among others (Robertson *et al.* 2013, Gonzalo Tampier and Grueter 2017). In Chile, wave energy is considered to have high potential, both in the mid and long term. Notwithstanding, the adaptation of wave energy technologies to the local conditions of the Chilean coast is still in a very early stage of development, which needs to be addressed by R&D and industrial innovation processes (Tampier and Zilic 2018).

On a global scale, current challenges for wave energy converter technologies are to prove reliability, to improve cost-effectiveness and to minimize environmental impact of WEC arrays (Astariz and Iglesias 2015, Iglesias *et al.* 2018). Nonetheless, their application in new locations, such as the Chilean coast, needs design adaptations to cope with the local environment (including natural hazards) and the limitations related to local manufacturing, installation, and maintenance capacities.

From a preliminary analysis, these local conditions should have an important effect in the selection of suitable WEC designs to minimize risks related to extreme events, minimize downtime

*Corresponding author, Ph.D. Student, E-mail: ignacio.pregnanjohannesen@plymouth.ac.uk

related to access for maintenance and minimize costs, avoiding services such as large floating cranes or DP (dynamic positioning) vessels. All these considerations are still under study and the present paper aims at making a first contribution to the analysis of extreme events at a location in southern Chile.

Extreme events are highly relevant to achieve a better understanding of possible limit states to be considered in the design and evaluation of floating structures in waves. For this purpose, different alternatives have been proposed in the last decades, as described in Klein *et al.* (2016). These include, among others, experiments or numerical simulations in regular and irregular waves considering extreme wave heights, design wave concepts (Adegeest *et al.* 2000, Dietz 2004, Friis-Hansen and Nielsen 1995, Torhaug *et al.* 1998, Tromans *et al.* 1991) or real-world extreme wave reproductions (Clauss *et al.* 2006, Fonseca *et al.* 2006, 2008, Schmittner 2005, Schmittner and Hennig 2012). Several investigations have been made regarding the impact of extreme waves on marine structures. For offshore structures with tubular members, reference is made to Clauss *et al.* (2010); Clauss *et al.* (2010), Gorf *et al.* (2000), Karunakaran *et al.* (1998), Suyuthi and Haver, (2009). For investigations related specifically to WEC technologies under extreme wave conditions, several investigations can be mentioned. In Yu and Li (2011), a preliminary study on the hydrodynamics of a WEC under extreme wave conditions is presented. Recently, Sirigu *et al.* (2020) have carried out an experimental campaign on a 1:20 scaled prototype of the ISWEC (Inertial Sea Wave Energy Converter), focusing on the influence of the mooring layout on loads in extreme wave conditions. Moreover, numerical methods have been widely applied to study the hydrodynamics performance of WECs. In Ransley *et al.* (2013, 2017), a numerical and physical model of extreme waves at Wave Hub, with a 100-year return period and a deterministic extreme wave was analyzed. In Ghasemi *et al.*, (2017), surge forces are numerically characterized for two different wave energy converters and in van Rij *et al.* (2019), a study to determine design loads for wave energy converters at various stages of the design process is presented. Heras *et al.* (2019) presents an investigation using potential theory, including non-linear forces in order to increase accuracy without losing computational efficiency. In the study, non-linear forces, hydrostatic restoring stiffness and different formulations of excitation forces and quadratic drag forces were included. Based on a numerical comparison, it is concluded that the different non-linear forces, except for the quadratic drag force, have a minor influence on the calculated motion of the pitching body. Many other investigations have been carried out for WECs and their response in waves. In Saincher and Banerjee (2016), a review about the influence of wave breaking on WEC hydrodynamics is presented and in Windt *et al.* (2018), the use of CFD as numerical wave tank is reviewed.

Considering the current development status of wave energy technologies, it can be assumed that not all technology types or categories (e.g., according to the eight categories identified by EMEC, European Marine Energy Centre) will be suitable for application in Chile.

The reasons for this may be related to extreme events, limitations due to unsuitable resources for manufacturing, installation or maintenance, or costs.

In the present paper, the experimental and numerical hydrodynamic assessment of a generic wave energy converter (WEC) under local extreme conditions is addressed, advancing the understanding of WECs survivability under Chilean environmental conditions. For this purpose, the analysis was performed taking two extreme conditions into account, for a potential deployment site in southern Chile: a 100-year return period sea state as reported in Lucero *et al.* (2017), and a deterministic focused wave.

On the other hand, this work provides useful benchmark data, which allow the validation of further numerical simulation methods. In addition, a comparison of two numerical methods (RANS

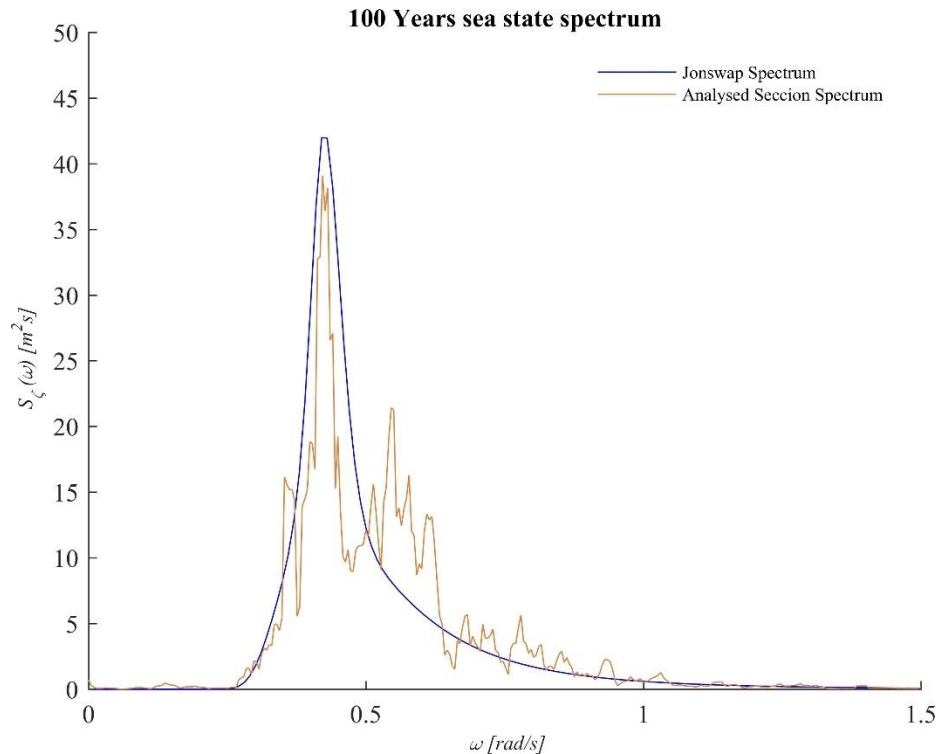


Fig. 1 Full scale case 1, theoretical and experimental measured spectra

Table 1 Properties of selected wave conditions for 100-year return period

Location (Lat. – Lon.)	40°00'21.9"S	73°48'22.1"W
Property	Value	Unit
H_s	9.65	<i>m</i>
T_p	14.81	<i>s</i>
Duration	3	<i>h</i>

CFD and potential panel method), for a viscous and inviscid flow respectively is presented, studying the accuracy and applicability of each method on WECs under extreme conditions.

2. Design waves

The survivability of a wave energy device is determined by its response in conditions that are sporadic and rare to witness. Therefore, the definition of those conditions plays a key role in the design process and will depend on several factors such as available environmental data, existing rules, previous experiences, design philosophy, among other aspects. In many cases, these conditions are defined as the worst sea condition for a defined return period (usually ranging from 25 to 100 years, e.g., Api 2005). Considering that these extreme sea states are a statistical representation, deterministic extreme wave conditions such as rogue waves are not included. Therefore, additional

deterministic experiments or simulations should be considered in the design process if such conditions are of interest. In the present investigation, an extreme sea state with a 100-year return period and a scaled reproduction of an extreme wave event are selected as extreme wave conditions for a selected location off the southern Chilean coast, to compare results from different analysis methods and discuss their suitability for future applications.

2.1 Case 1: 100-year return period sea state

Table 1 presents the characteristics of a 100-year sea state for a selected location in Punta Galera, off the coast of Valdivia, southern Chile, obtained from the data presented in Lucero *et al.* (2017). At this position, rough weather and high energy conditions are common over the year.

The values of peak period (T_p) and significant wave height (H_s) for the 100-year return period were used to create a JONSWAP (Joint North Sea Wave Observation Project) spectrum, with $\gamma = 3.3$. In Fig. 1, the theoretical and the experimentally measured spectra are compared in full scale.

2.2 Case 2: Focused wave

Different definitions for a “Freak Wave” or “Rogue Wave” are found in literature, such as $H_{max} \geq 2.4 \cdot H_s$, from Faulkner (2000) and $H_{max} \geq 2.3 \cdot H_s$ from Wolfram *et al.* (2000). However, there is consensus among researchers that the maximum wave height is at least twice as high as the significant wave height: $H_{max} \geq 2 \cdot H_s$ as stated in (Kharif *et al.* 2009).

In the present investigation, a focused wave with $H_{max} = 8.4 \text{ m}$ was generated, mainly due to technical restrictions of the experimental setup and the maximum possible wave height limits imposed by the wave generator for focused waves.

Considering this maximum wave height, the corresponding significant wave height was defined to achieve $H_{max} = 2 \cdot H_s$. Then, the significant wave height results in $H_s = 4.2 \text{ m}$. Although this significant wave height is not necessarily a worst-case scenario, the achieved maximum wave height can be considered as a valid extreme wave case, which may serve as a benchmark for future simulations or experiments in other facilities. The final profile of the focused wave is shown in section 4.3, Fig. 6.

3. Experimental methodology

3.1 Experimental setup

Model tests of the WEC model were conducted in the seakeeping basin at Technical University Berlin, Germany. The basin, shown in Fig. 2, is 120 m long and 8 m wide with a water depth of 1 m. It is equipped with an electrically driven wave maker for the generation of tailored, deterministic irregular sea states. The model was constructed from wood with a cover of fiber reinforced glass. The scaling process was conducted by the Froude method with a factor of 1:70. The buoy consists of a cylindrical floater with a hemispherical bottom, as can be seen in Fig. 3. The main dimensions of the setup are summarized in Tables 2 and 3.

The current study does not incorporate a power take-off (PTO) damping system. Since this research employs a generic WEC design for hydrodynamic analysis, specific considerations regarding a PTO system design for the full-scale model are not taken into account. However,

previous investigations involving the same WEC model have been conducted both experimentally and numerically in regular waves, using a hydraulic PTO system with varying damping ratios, as described in Tampier and Grueter (2017).



Fig. 2 Technical University Berlin wave tank

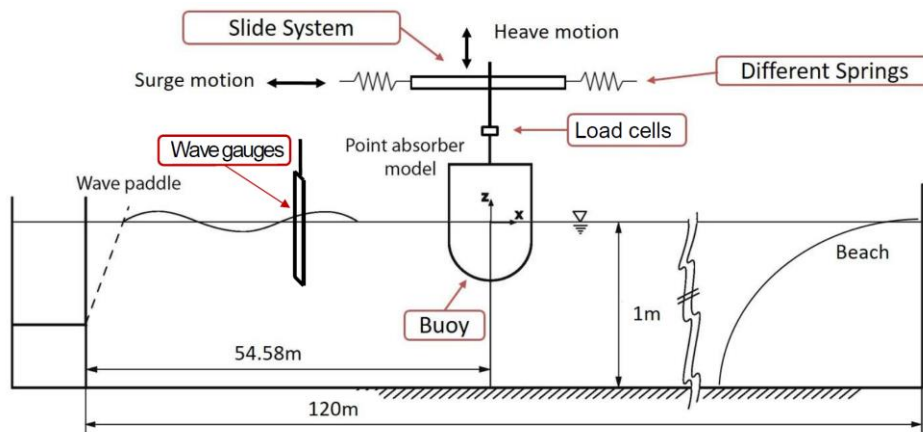


Fig. 3 Experimental setup at the basin

Table 2 Characteristics of the seakeeping basin at TU-Berlin

Wave tank		
Length	120	<i>m</i>
Width	8	<i>m</i>
Water depth	1	<i>m</i>
Max. wave frequency	13	<i>rad/s</i>
Max. wave height	0.35	<i>m</i>
Length	120	<i>m</i>
Width	8	<i>m</i>
Water depth	1	<i>m</i>

Table 3 Main dimensions of the generic WEC

	Full scale		Model scale	
Diameter D	28	<i>m</i>	0.4	<i>m</i>
Draft T	21	<i>m</i>	0.3	<i>m</i>
Freeboard FB	7	<i>m</i>	0.1	<i>m</i>
Scale λ			70	

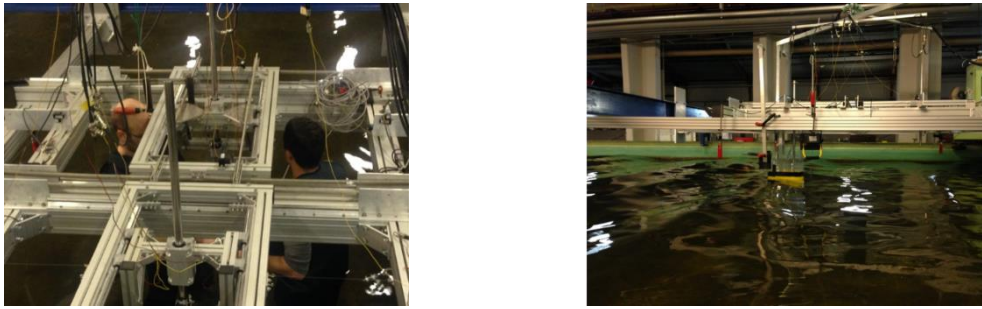


Fig. 4 Technical University Berlin wave tank

The Experimental setup is shown in Fig. 3 and the test rig installed in the wave tank is shown in Fig. 4.

At a first stage, wave tests without the generic WEC were made to obtain undisturbed wave profiles. For these experiments, a wave gauge was located 54.58 m from the wave paddle, the same position to be used by the WEC. For the second part of the experiments, with the WEC installed, a wave gauge was installed 2.5 m before the WEC (52.08 m from the wave paddle) and a second one parallel to the WEC (54.58 m from the wave paddle), 2 m sideways.

The WEC is connected to a measuring frame with two rods, which are guided by linear bearings. The measuring frame consists of a sliding system, which allows movements of the model in all translational directions; although, for this work, only surge and heave motion were permitted. To avoid coupled results, a simplification in the mooring system was used. Springs were attached to the frame in the x direction, representing a mooring system which applies only horizontal forces (i.e., a mooring system with auxiliary buoys).

For the measurement of forces, two six-component load cells were installed at the connecting rods. For the measurement of surge and heave motions, a series of resistive distance sensors were used at the frame.

4. Numerical methodology

4.1 Governing equations

In the present work, the governing equations of an incompressible, viscous laminar flow are described by the equations of mass and momentum conservation as presented in index notation form (Ferziger *et al.* 2020) in Eqs. (1) and (2), respectively

$$\frac{\partial u_i}{\partial x_i} = 0 \quad (1)$$

$$\rho \left(\frac{\partial u_i}{\partial t} + u_j \frac{\partial u_i}{\partial x_j} \right) = -\frac{\partial P}{\partial x_i} + \mu \frac{\partial^2 u_i}{\partial x_j \partial x_j} - \rho f_i \quad (2)$$

With the position vector x , flow velocity u , dynamic viscosity μ , density ρ , pressure P and an external force f . In Eq. (2), the right-hand side represents the field pressure gradient, frictional force due to the laminar boundary layer and the external body force. On left hand side, the total acceleration of an irrotational flow in Euler coordinates is represented. Since a laminar flow is considered, the set of Eqs. (1) and (2) is closed and can be solved by applying the finite volume method without a turbulent model.

In addition, The VOF (Volume of Fluid) method is used to compute the free surface, if the immiscible fluid phases in a single volume have the same velocity, pressure, and temperature fields. In consequence, the governing equations are the same as those in a single-phase flow, in which fluid properties are defined as follows

$$\rho = \sum_i \rho_i a_i \quad (3)$$

$$\mu = \sum_i \mu_i a_i \quad (4)$$

$$\sum_i a_i = 1 \quad (5)$$

Where $a_i = \frac{V_i}{V}$ is the volume fraction of the i^{th} phase.

NEMOH is the linear potential flow solver used in this research. The governing equations are the Laplace (6) and Lagrange (7) equations which are then linearized using a perturbation series, as described by Delhommeau (1989)

$$\left(\frac{\partial^2 \phi}{\partial x_i^2} \right) = 0 \quad (6)$$

$$\left(\frac{\partial \phi}{\partial t} \right) + \frac{1}{2} \left(\frac{\partial \phi}{\partial x_i} \right)^2 + \frac{p}{\rho} + gz = F(t) \quad (7)$$

Here, g is the gravitational acceleration, z is the vertical coordinate, $F(t)$ is an arbitrary function of time and ϕ is the potential flow function, defined as

$$u_i = \frac{\partial \phi}{\partial x_i} \quad (8)$$

4.2 Floating body motions

To capture the motions of a floating device, Newton's second law is applied to the inertial body mass, considering the hydrodynamics and external forces, with the following formulation

$$m_{ij} \ddot{s}_i = F_{rad} + F_w + F_{fr} + F_{ext} \quad (9)$$

Where, i refers to the direction of action and j to the direction of motion caused by the respective force component. m_{ij} is the mass of the body, \ddot{s} is the body acceleration. F_{rad} , F_w , F_{fr} and F_{ext} are the radiation, wave, friction due to boundary layer and external forces, respectively. In Computational Fluid Dynamics (CFD) based on the finite volume method, the right-hand side of Eq. (9) is the total summation of hydrodynamic and external forces. The body motion is obtained by the numerical solution of Eq. (9).

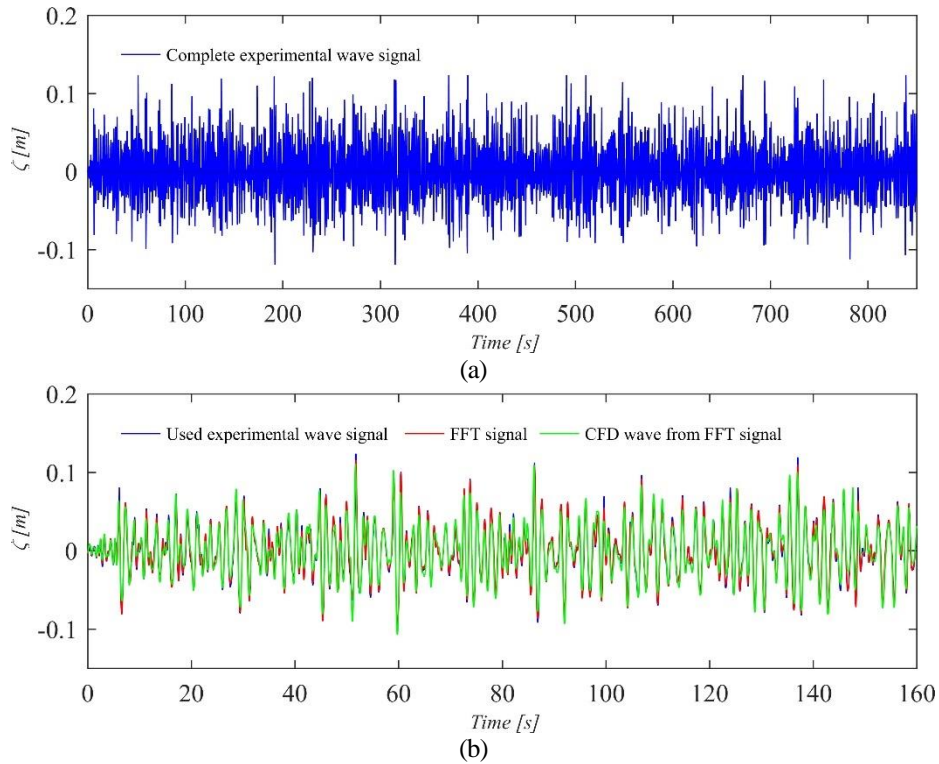


Fig. 5 experimental (a) and selected detail (b) of the time series of the 100-year return period sea state (case 1) at model scale

In the case of the potential method, body dynamics Eq. (9), written in index notation, becomes

$$\sum_{i,j=1}^6 [(m_{ij} + a_{ij})\ddot{s}_i + b_{ij}\dot{s}_i + c_{ij}s_i] = F_{ex.i} \quad (10)$$

Where, s is the motion of the body, \dot{s} is the body's velocity a_{ij} is the added mass, b_{ij} is the total linear damping coefficient, including potential hydrodynamic and internal and external viscous effects, c_{ij} is the total external and hydrodynamic restoring coefficient, and $F_{ex.i}$ is the incident and diffraction waves excitation force on the device. Solving Eq. (10) for s_i and dividing s_i by the wave amplitude η , the RAOs for the six degrees of freedom are obtained.

The analysis was carried out for two degrees of freedom, namely surge and heave, neglecting coupled effects.

4.3 Numerical wave pre-processing

The aim of the present work is to carry out a comparison between experimental and numerical methods. To achieve a suitable comparison, numerical simulations are set-up using measured wave elevation time series from experiments as input data. Therefore, the numerical wave signal is a deterministic reproduction of the measured stochastic waves from experimental tests.

In RANS and panel methods, the wave elevation input data $\eta(t)$ are a summation of linear components of the measured wave. Represented by a Fourier series, the input wave defined by

Table 4 Comparison of spectral wave parameters

	CFD		Experimental	
Spectral moment m_0	0.001079	m ²	0.001188	m ²
Sign. wave height $H_{1/3}$	0.1314	m	0.1379	m
Mean period T_m	1.499	s	1.770	s

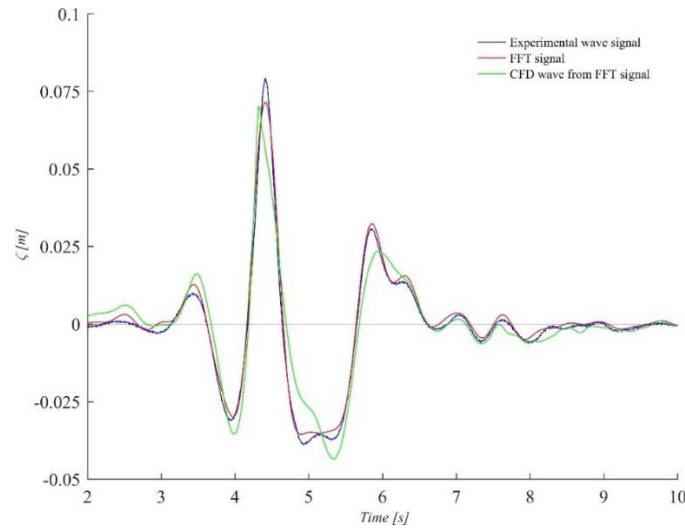


Fig. 6 Focused wave (case2) time series for different methods at model scale

Bhattacharya (1978) is

$$\eta(t) = \sum_{j=1}^n \eta(j) \sin(\omega(j)t + \varphi_W(j)) \quad (11)$$

Where, j refers to the wave component in the Fourier series, $\eta(j)$, $\omega(j)$ and $\varphi_W(j)$ are amplitude, frequency, and phase respectively for each linear wave component. To compute the variables, Fast Fourier Transform (FFT) was applied to the experimental wave signal.

Due to computation time constraints, the numerical simulations were limited to a selected time section of the experimental data. The selected section contains relevant stochastic information of the generated wave. In case of the 100-year storm, Fig. 5(a) shows the experimental wave signal, while Fig. 5(b) shows the selected section, comparing experimental and FFT signals. Both corresponding spectra shown in Fig. 1. In case of the focused wave, Fig. 6 shows experimental and FFT signals for the simulated wave. From the figure, can be observed that the selected data shows similar wave amplitude distribution, as a pattern along the complete wave signal. In Table 4, spectral parameters are given.

4.4 Numerical wave pre-processing

4.4.1 RANS CFD setup

RANS CFD computations were carried out using the Siemens STAR-CCM+ software, defining

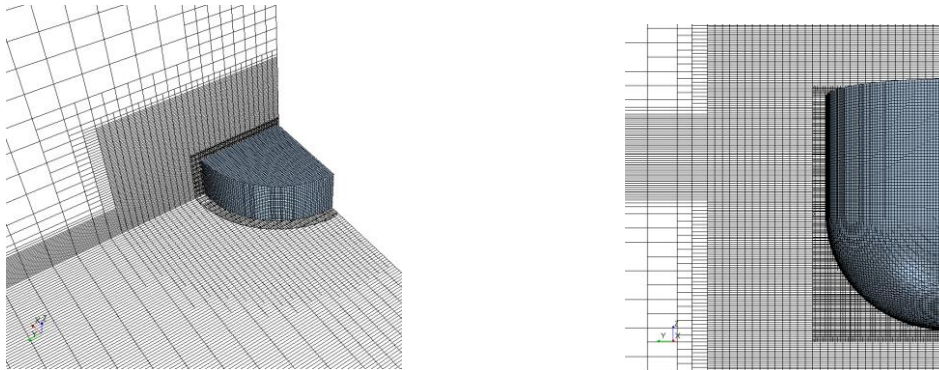


Fig. 7 CFD mesh and refinement details

Table 5 Mesh parameters for free surface region

100-year return period storm mesh			Focused wave mesh		
N° per λ	54		N° per λ	56	
N° per H	15		N° per H	25	
Aspect ratio	$z : x$	$z : y$	Aspect ratio	$z : x$	$z : y$
	1:1.25	1:2.17		1:1.75	1:4.17

a numerical wave tank, replicating the used experimental setup and as continuation of the previous work carried out by Pregnan and Tampier (2018).

Simulations were configured with an implicit unsteady time integration scheme. The inlet boundary conditions are the equations that define the surface elevation and the velocities by the VOF wave model. In the downstream free-surface area, a Volume of Fluid (VOF) damping technique was incorporated using a STAR-CCM+ built-in function. This approach involves introducing a resistance term to the vertical motion of the free surface (in the z direction), as formulated by Choi and Yoon (2009). In addition, a gradually decreasing discretization resolution was applied to further reduce wave amplitudes, preventing unwanted wave reflections. On the other hand, in the upstream area, it was not possible to apply a damping free-surface condition for the radiation waves generated by the buoy motion, since it would also impact on the numerically generated wave train. The proximity of the inlet boundary could lead to reflection of the radiation waves. However, due to limited computational resources and the refined free-surface region situated between the inlet and closely after the buoy, it was necessary to decrease the inlet-buoy distance. In Addition, it is expected that the impact of radiation waves on the inlet boundary can be assumed negligible.

A symmetrical plane condition was applied in the x - z plane of the tank, simulating only half of the basin and the buoy. The device was configured with a non-slip wall condition and placed in an overset region into the tank domain.

To save computational resources, laminar flow was considered in all simulations. This allows for a coarser mesh near the body, and no-turbulence model.

The numerical setup has the same cross section as the experimental setup (see Table 2), nonetheless only considering 2 m upstream and 8 m downstream. The mesh was designed taking ITTC Recommended Procedures and Guidelines (2014) into account. As seen in Fig. 7 (left), a continuous cell size was configured along the free surface region. To allow the motion of the body,

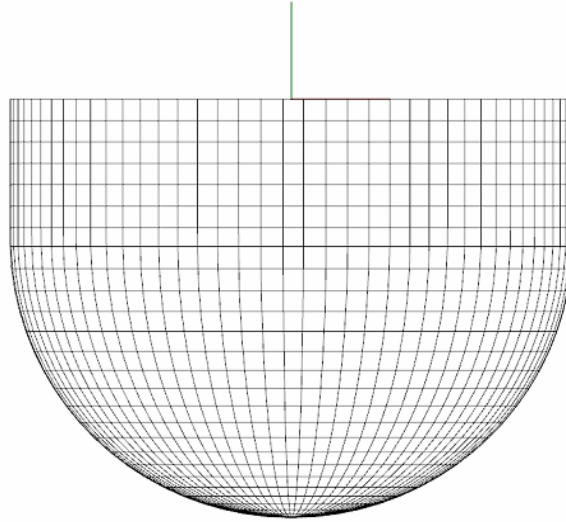


Fig. 8 Generated panel mesh

an overset mesh was applied in the domain as shown in Fig. 7 (left and right). The domain was meshed with polyhedral elements, with refinements using hexahedral elements. Table 5 shows the main parameters of the mesh in terms of wavelength (λ) and wave height (H). This configuration represents approximately 1.2M cells for case 1 and approximately 2.6M cells for case 2.

As previously mentioned, experiments and simulations only considered heave and surge motions. To restrain surge in the system, as described in section 3.1, a spring force in x direction was applied, equivalent to the experimental setup.

4.4.2 Panel code setup

As presented in Eq. (10), the model is restricted to simulating the behavior of the wave energy converter device in frequency domain. Nevertheless, as mentioned previously in section 4.3, Fourier series can be applied on a general periodic wave train, expanding the method to consider irregular waves.

The device response in the time domain is calculated by the sum of each linear response component calculated with a Fourier analysis by Eq. (10) in discrete form as

$$s_i(t) = \sum_{j=1}^n H_i(\omega(j)) \eta(j) \sin(\omega(j)t + \varphi_W(j) - \varphi_R(j)) \quad (12)$$

Here, i is the number of the motion and j is the wave component in the Fourier series. To perform the sum in Eq. (12), added mass, damping and restoration coefficient, as well as diffraction and incident wave force in Eq. (9) were calculated by NEMOH. In Addition, the experimental mooring configuration was added to the system as a linear spring force with the stiffness corresponding to the restoring coefficient C_{11} . Subsequently, obtaining the corresponding uncoupled Response Amplitude Operators $H_i(\omega(j))$ and response phase $\varphi_R(j)$.

The panel mesh used in NEMOH is shown in Fig. 8, composed by 1027 elements.

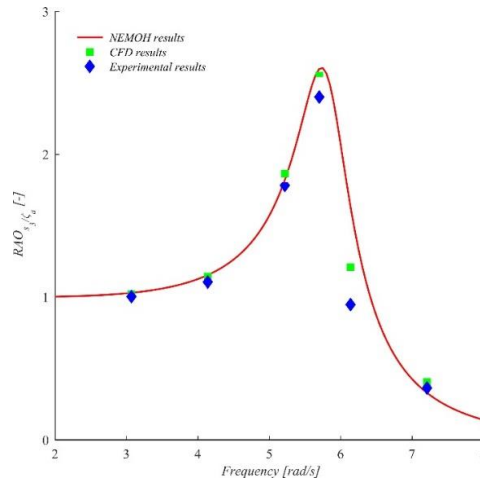


Fig. 9 Heave RAOs obtained by the different methods at model scale

Table 6 Heave RAOs from experiments, potential model and CFD simulations

Frequency ω (rad/s)	Experimental (-)	Potential (-)	CFD (-)
3.07	1.01	1.03	1.02
4.14	1.11	1.16	1.06
5.22	1.77	1.82	1.86
5.70	2.40	2.60	2.56
6.14	0.95	1.61	1.21
7.21	0.36	0.33	0.40

5. Results

5.1 Response in regular waves

To assess the accuracy of the applied methods, the heave RAOs were computed and compared with previous research Pregnan and Tampier (2018); Tampier and Grueter (2017). Additionally, the external damping, generated by the bearings and rods of the frame on the experimental setup, was considered by an empirical correction of the b_{11} coefficient. The b_{11} correction was achieved by comparing the numerical and experimental surge free-decay test, to then apply the corrected coefficient into the numerical irregular wave analysis.

Results can be seen in Fig. 9 and Table 6, showing good agreement. However, near to the resonance frequency, differences can be observed due to the nature of the formulations, which consider a linear viscous coefficient for the potential and RANS methods.

5.2 Response in irregular waves

The heave and surge time series, as shown in Figs. 10 and 11, compare the panel and CFD methods with experimental results. As Fig. 10 (top) shows, heave response among methods is similar,

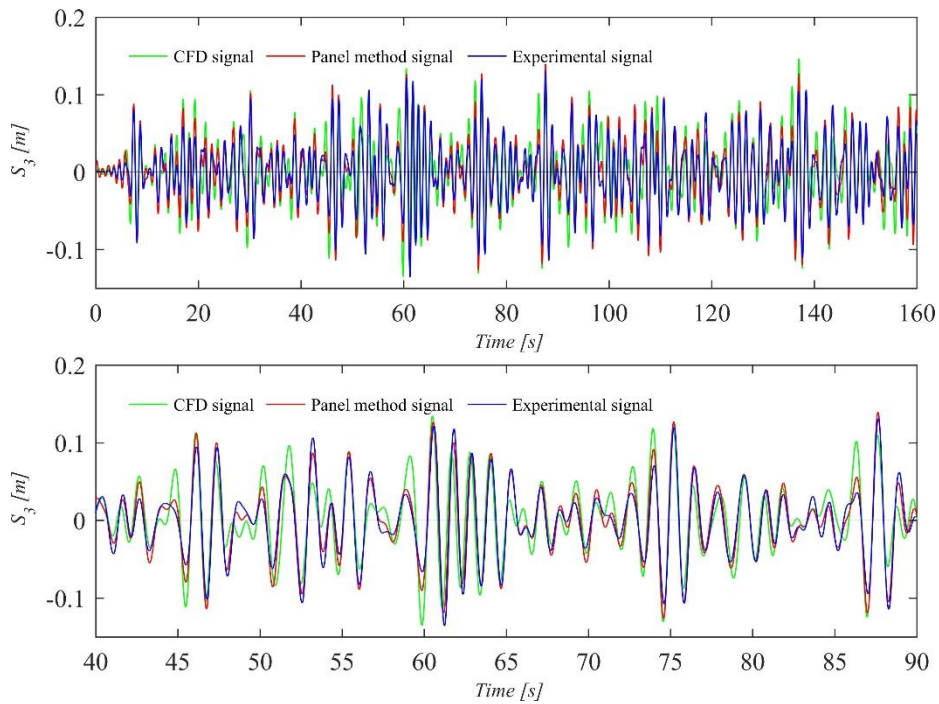


Fig. 10 100-year sea state heave response at model scale

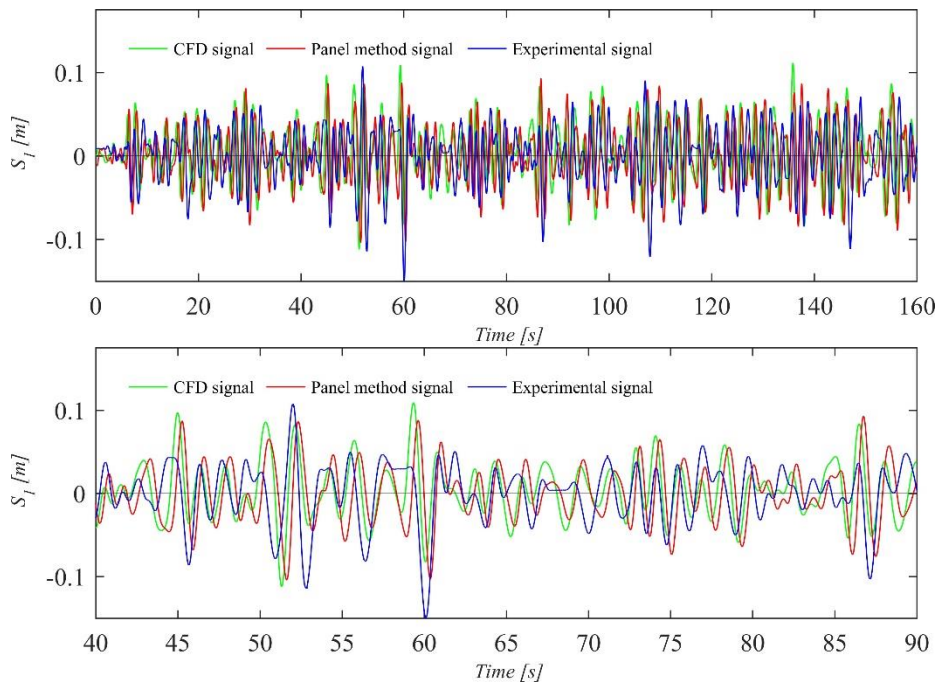


Fig. 11 100-year sea state surge response at model scale

showing good agreement between numerical and experimental results. In Fig. 10 (bottom), a closer look between 40 and 90 seconds is shown. Here, extreme events take place, in which the highest wave amplitudes for the analyzed time series appear. In this section, the highest amplitudes of the body motions are observed. Both numerical methods reproduce the response of the body with good agreement to experiments at extreme events. Nevertheless, both numerical methods calculated higher amplitudes than those found in the experimental data. Especially CFD simulations present the largest deviations, overestimating the heave response. On the other hand, the panel method shows smaller deviations, even in the highest wave near the 90-second mark.

Regarding the surge response (Fig. 11), the numerical simulations were able to capture the behavior, showing an acceptable agreement between them and with the experimental results, in

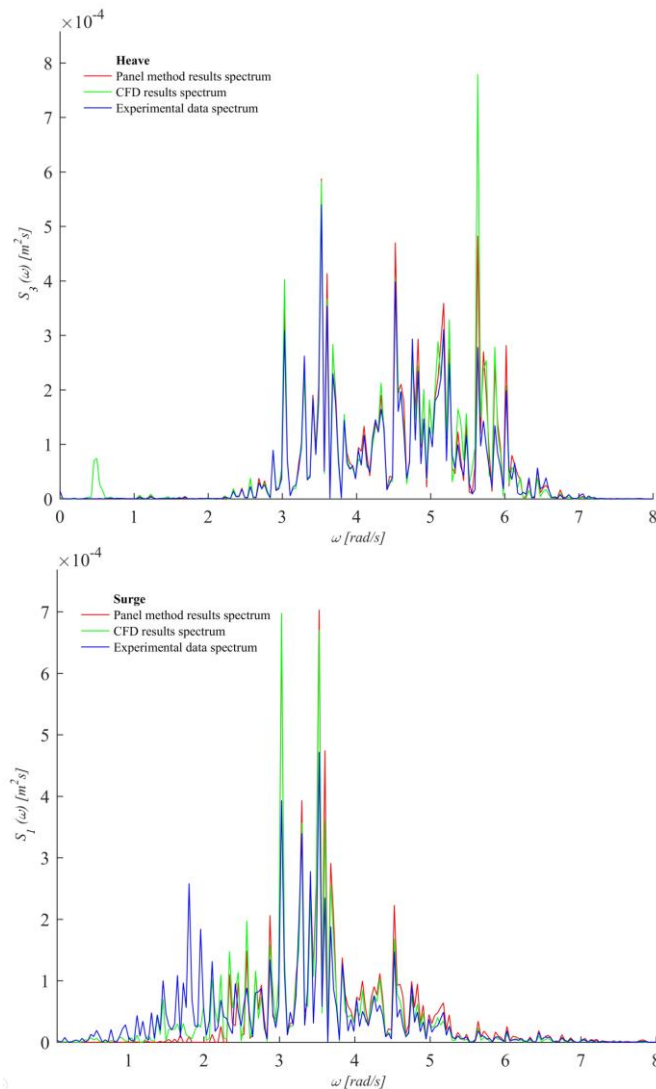


Fig. 12 Motion response spectrums at model scale: Heave response spectrum (top) and surge response spectrum (bottom)

Table 7 Comparison of spectral parameters between different methods

Motion	Parameter	Panel method		CFD		Experimental	
		Value	Unit	Value	Unit	Value	Unit
Heave	Spectral moment m_{03}	0.00184	m^2	0.00188	m^2	0.00155	m^2
	Significant response S_3	0.0857	m	0.0867	m	0.0788	m
	Mean period T_m	1.3680	s	1.3823	s	1.3922	s
Surge	Spectral moment m_{01}	0.00124	m^2	0.00123	m^2	0.00123	m^2
	Significant response S_1	0.0704	m	0.0702	m	0.0702	m
	Mean period T_m	1.6727	s	1.8600	s	2.1992	s

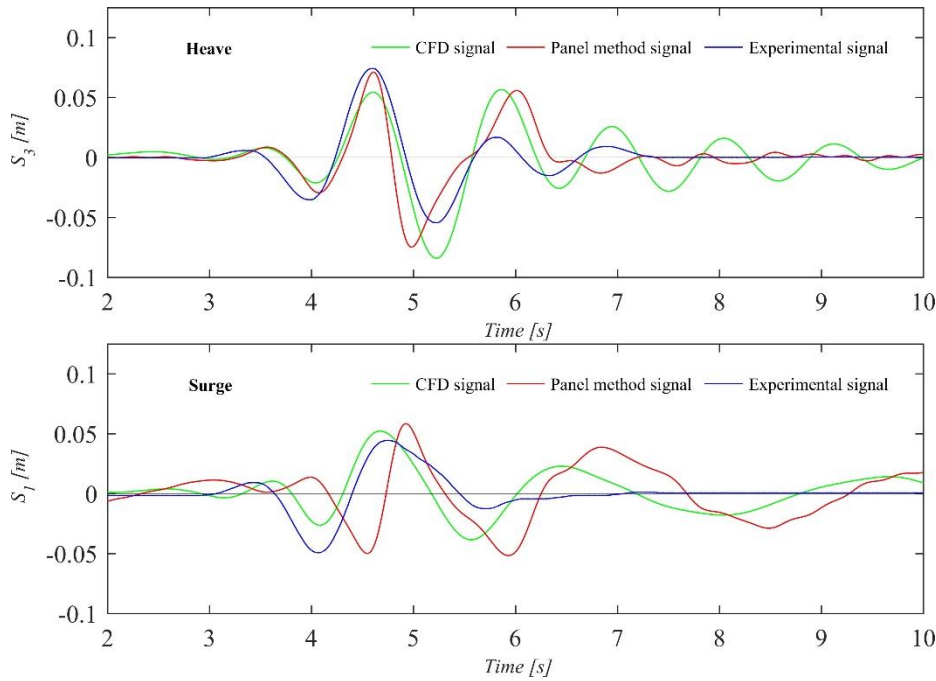


Fig. 13 Focused wave response in the three methods

which the CFD simulation shows better agreement. Regarding the amplitude of the response, some differences can be observed. Both numerical methods overestimate the response, especially near the peak values. For the phase response, the panel method presents a clear delay compared to the CFD and experimental signal.

Additionally, a spectrum analysis of the time series has been carried out. The response spectra are presented in Fig. 12 and a comparison of the main spectral parameters is shown in Table 7. The results for the significant response and mean period show that even with some differences, numerical results show a similar statistical behavior compared to experimental data.

For the heave spectrum, in Fig. 12 (top), a slight difference in the significant response between potential and RANS methods can be observed, overestimating experimental results. This is consistent with the time domain analysis. From the plots it can also be deduced that the total amount

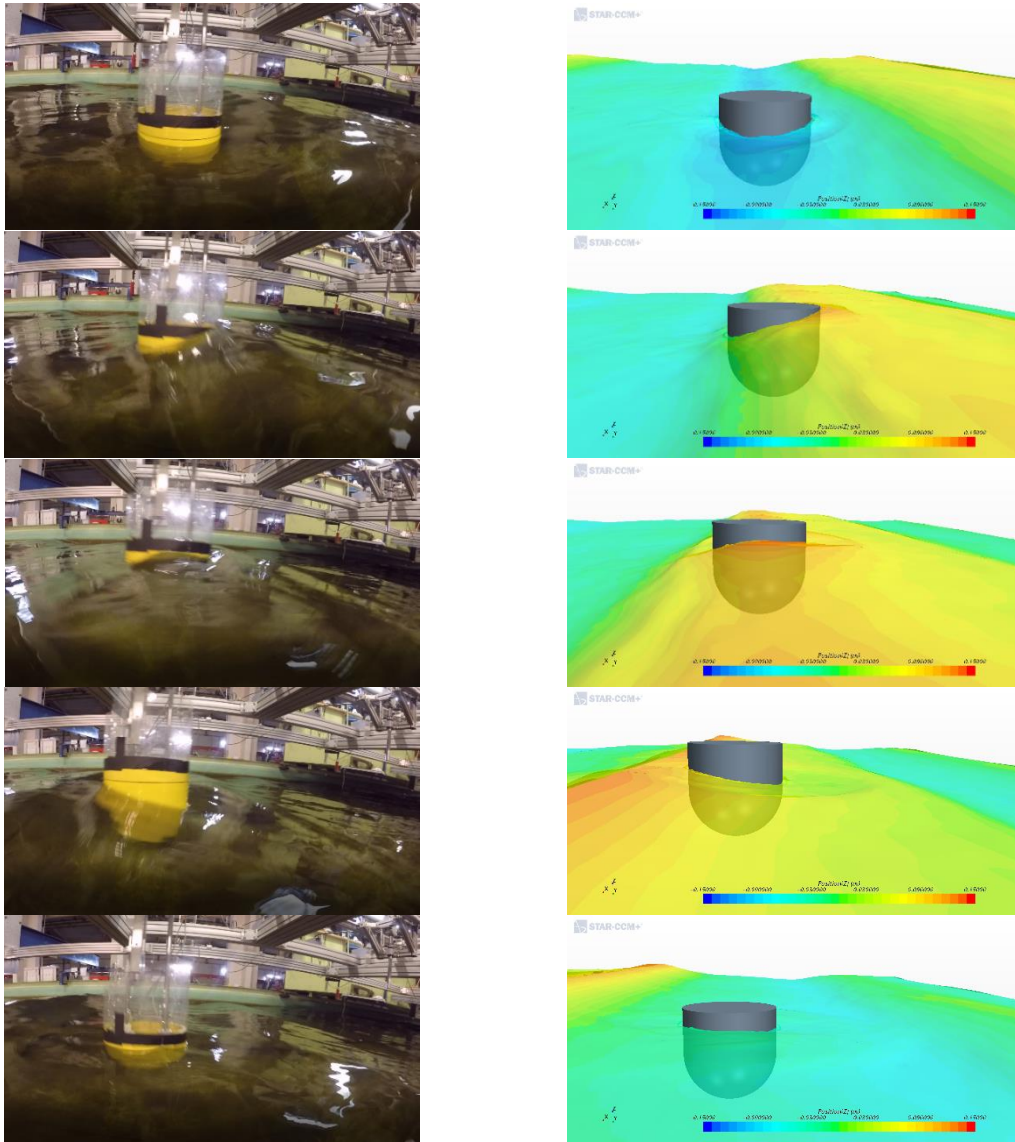


Fig. 14 Example of the experimental and numerical response of the device in irregular waves..

of energy for both numerical methods correlate well with the experimental data. For the surge spectrum, the mean periods calculated by both numerical methods show the main differences, underestimating the magnitude compared to the experimental values. Considering parameters in Table 7 (spectral moments, significant response amplitude and mean period), it is observed that the CFD and potential methods show good agreement with experimental data, being consistent with the previous analysis in the time domain.

Furthermore, the surge response spectrum shows a low frequency band from 1 to 2 rad/s, that appears to be a sub-harmonic of the peak frequency between 3.5 and 4 rad/s, representing second order forces which might play a relevant role for surge. This is not observed for the heave motion.

From Fig. 12 (bottom), it can be observed that this low frequency effect at surge is weakly captured by the CFD simulations, compared to experimental results. For the panel method, which was limited to linear forces, surge responses at low frequencies are practically negligible. This could be improved by the implementation of second order drag forces in the future.

5.3 Focused wave

Fig. 13 shows the time series of heave and surge responses in a focused wave, calculated by the panel and the RANS method, and compared to the experimental data. Considering that this is a highly non-linear extreme event, both methods show good agreement for the response of the system.

For the heave response, both numerical methods show similar results and good agreement with the experimental data. Differences in the amplitude of the response were expected due to the differences in the shape of the exciting waves for the different methods (Fig. 6). Although, much better agreement is found for the exciting wave signals (Fig. 6), than for the body responses (Fig. 13, top).

For the surge response, larger deviations between the single numerical methods can be observed. Here, RANS results show better agreement with the experimental data, whereas the panel code shows large discrepancies for the motion amplitude and the phase response.

To observe the response of the body in an extreme sea state in detail, Fig. 14 shows a selected sequence of visualization (53 to 54 s, in 0.2s steps) from RANS simulations and experiments. It can be seen that RANS simulations reproduce the physical phenomena satisfactorily, both for the free surface and the motions.

6. Discussion

Numerical simulations show good correlation against experimental data for the cases of the analyzed irregular sea state and the focused wave. For the heave motion, both, panel, and RANS methods correlate well with the experimental data, which is expected due to the freedom of the heave motion in the experimental setup. In contrast, the surge motion in the experimental setup is restricted by a mooring system consisting of linear springs, which is mimicked in the numerical setups. Although the friction effects of the bearings and rods were accounted for, adding a linear coefficient to the surge response, it can be inferred that the frame system behavior is not completely linear along its load cycles. This can explain the partly large differences of the numerical results with respect to the experimental data, particularly for peak responses as shown in Fig. 11.

One of the main differences between both numerical methods is the calculation domain. While the RANS method simulates the fluid and body behavior in the time domain, using all the excitation forces related to free surface deformation to calculate the body response, the panel method uses a Fourier transform to move from frequency to time domain. Due to the neglected coupled effects in the frequency domain, motions are uncoupled and not affected by other external conditions, such as the surge restrictions. Therefore, the buoy is exposed to a slightly different encounter frequency with the waves, comparing RANS and experimental data. Besides, the phase response in the potential method has an accumulative error, possibly due to some mismatching with the excitation frequency.

The differences in the mean surge period, observed in the spectral analysis of the response in irregular sea state conditions, might be a result of the different damping coefficients from each method, which lead to a shift in the response period. Results are consistent given that the potential

code does not consider viscous effects; while the RANS method considers viscous effects, although only in the laminar range. The RANS setup is thus closer to the experimental condition, giving a better approximation.

Some of the inaccuracies of the RANS method that arise in the irregular wave and are more noticeable in the focused wave simulations are related to the input surface elevation. As seen in figure 6, the numerical input wave signals deviate from the measured wave signals, which may partially explain the response disparities of the numerically obtained heave and surge motions compared to experimental data. The correct simulation of a deterministic wave is a complex problem, which is not easy to solve. On the other hand, the wave input for the panel method corresponds to the FFT signal (Fig. 6), only depending on the correct transformation of the experimental signal to a Fourier series (Eq. (11)).

Based on the obtained results, for simple geometry, such as the one used in this study, the presented panel code and FFT methodology can be recommended for early engineering stages. The use of a panel method in non-breaking wave conditions can help to identify critical events and the corresponding response of the floater. In a second stage, RANS simulations of selected critical events can help to determine the response of the floater under extreme conditions and provide input for a more detailed design of the mooring system.

It is important to mention that these results are only applicable for devices of similar geometry. Due to the regular and compact shape of the buoy analyzed in this work, no high turbulence effects in the degrees of freedom that are allowed develop; thus, making the geometry a good candidate for a potential method analysis, even in non-linear conditions.

7. Conclusions

In extreme sea states, i.e., a 100-year storm and a focused wave, a selected portion of the storm wave elevation time series was simulated by two numerical methods and compared with experimental data, showing close correlation. The spectra of response were also calculated, showing good agreement in the total amount of energy and mean frequency of the motions.

The focused wave simulation showed the largest differences between the methods. Here, RANS results showed better agreement with measurements for heave and surge responses. The potential method achieved good results only for the heave motion, not being able to characterize the surge response of the floater.

Generally, it may be concluded, that both numerical methods achieve similar results in irregular waves, being useful for first stages of the floater and the mooring design.

Results showed that the panel method is a valuable tool for the response analyses in regular and irregular sea states, mainly due to the considerably lower required computational resources. Although an accurate reproduction of the deterministic incident wave can be achieved, discrepancies were observed for the body responses, especially for surge motions. On the other hand, the RANS method showed good capabilities for the simulation of higher order effects in heave and surge responses. However, the main difficulty of the method was associated with the correct reproduction of the deterministic wave elevation. This will be addressed in future investigations with an automated iterative approach.

With the achieved results and considering only geometries similar to the one studied in this work, it is possible to propose this methodology of analysis for early design stages, considering a panel method and FFT post-processing, and subsequently, use the data for selected RANS simulations of

extreme conditions.

Additional future research in this field is being considered. The analysis of other geometries (i.e. other WEC categories) is expected to provide a better understanding of the capabilities and limitations of the analyzed methods. Besides, further studies including more complex loading conditions will be considered for different geometries and environmental conditions, including a more complex modeling of the mooring effects on the floating body.

Acknowledgements

Acknowledgement to the German Academic Exchange Service (DAAD) and the Marine Energy Research and Innovation Center (MERIC) for the partial funding of this investigation is given.

References

- Adegeest, L., Braathen, A. and Vada, T. (2000), "Evaluation of methods for estimation of extreme nonlinear ship responses based on numerical simulations and model tests", *Proceedings of the 22nd Symposium on Naval Hydrodynamics*.
- Astariz, S. and Iglesias, G. (2015), "The economics of wave energy: A review", *Renew. Sust. Energ. Rev.*, **45**, 397-408. <https://doi.org/10.1016/j.rser.2015.01.061>.
- Bhattacharya, R. (1978), *Dynamics of Marine Vehicles*.
- Choi, J. and Yoon, S.B. (2009), "Numerical simulations using momentum source wave-maker applied to RANS equation model", *Coast. Eng.*, **56**(10), 1043-1060. <https://doi.org/10.1016/j.coastaleng.2009.06.009>.
- Clauss, G.F., Haver, S. and Strach, M. (2010), "Breaking wave impacts on platform columns: Stochastic analysis and DNV recommended practice", *Proceedings of the ASME 2010 29th International Conference on Ocean, Offshore and Arctic Engineering*. <https://doi.org/10.1115/OMAE2010-20293>.
- Clauss, G., Schmittner, C. and Hennig, J. (2006), "Systematically varied rogue wave sequences for the experimental investigation of extreme structure behavior", *Proceedings of OMAE2006 25th International Conference on Offshore Mechanics and Arctic Engineering*.
- Clauss, Günther, Klein, M. and Dudek, M. (2010), "Influence of the bow shape on loads in high and steep waves", *Proceedings of the 29th International Conference on Ocean, Offshore and Arctic Engineering*, 1-12.
- Delhommeau, G. (1989), "Amélioration des performances des codes de calcul de diffraction-radiation au premier ordre", In *2nd Journées de l'hydrodynamique*, 70-86.
- Dietz, J.S. (2004), *Application of Conditional Waves as Critical Wave Episodes for Extreme Loads on Marine Structures* (Issue July), Technical University of Denmark.
- EMEC: European Marine Energy Centre (2003), <http://www.emec.org.uk/>
- Ferziger, J.H., Perić, M. and Street, R.L. (2020), *Computational methods for fluid dynamics*, Springer International Publishing. <https://doi.org/10.1007/978-3-319-99693-6>.
- Fonseca, N., Guedes Soares, C. and Pascoal, R. (2006), "Structural loads induced in a containership by abnormal wave conditions", *J. Mar. Sci. Technol.*, **11**(4), 245-259. <https://doi.org/10.1007/s00773-006-0222-9>.
- Fonseca, N., Pascoal, R. and Guedes Soares, C. (2008), "Global structural loads induced by abnormal waves and design storms on a FPSO", *J. Offshore Mech. Arct.*, **130**(2), 021005. <https://doi.org/10.1115/1.2779334>.
- Friis-Hansen, P. and Nielsen, L.P. (1995), "On the new wave model for the kinematics of large ocean waves", *OMAE 1995, Proceedings of the 14th Intl Conf on Offshore Mechanics & Arctic Engng*.
- Ghasemi, A., Anbarsooz, M., Malvandi, A. and Hedayati, F. (2017), "A nonlinear computational modeling of wave energy converters: A tethered point absorber and a bottom-hinged flap device", *Renew. Energ.*, **103**,

- 774-785. <https://doi.org/10.1016/j.renene.2016.11.011>.
- Gorf, P., Barltrop, N., Okan, B., Hodgson, T. and Rainey, R. (2000), FPSO bow damage in steep waves, *Rogue Waves 2000*.
- Heras, P., Thomas, S., Kramer, M. and Kofoed, J.P. (2019), “Numerical and experimental modelling of a wave energy converter pitching in close proximity to a fixed structure”, *J. Mar. Sci. Eng.*, **7**(7), 1-27. <https://doi.org/10.3390/jmse7070218>.
- Iglesias, G., Astariz, S. and Vazquez, A. (2018), “The economics of wave and tidal energy”, (Eds., D. Greaves and G. Iglesias), *Wave and Tidal Energy*, 513-532.
- ITTC (2014), *ITTC – Recommended Guidelines - Wave energy converter - Model test experiments 7.5-02-07-03.7 (Revision 01)*. 13.
- Karunakaran, D., Baerheim, M. and Spidsore, N. (1998), “Measure and Simulated dynamic response of a jacket and a large jack-up platform in North Sea”, *Proceedings of the 16th International Conference on Offshore Mechanics and Arctic Engineering*, Vol. II, May.
- Klein, M., Clauss, G.F., Rajendran, S., Soares, C.G. and Onorato, M. (2016), “Peregrine breathers as design waves for wave-structure interaction”, *Ocean Eng.*, **128**, 199-212. <https://doi.org/10.1016/j.oceaneng.2016.09.042>.
- Lucero, F., Catalán, P.A., Ossandón, Á., Beyá, J., Puelma, A. and Zamorano, L. (2017), “Wave energy assessment in the central-south coast of Chile”, *Renew. Energ.*, **114**, 120-131. <https://doi.org/10.1016/j.renene.2017.03.076>.
- Pregnan, I. and Tampier, G. (2018), “Simulation of motions and forces for a generic wave energy converter using RANS CFD”, (Ed., C. Guedes Soares), *Advances in Renewable Energies Offshore*, Taylor & Francis Group.
- Ransley, E., Hann, M., Greaves, D., Raby, A. and Simmonds, D. (2013), “Numerical and physical modeling of extreme waves at Wave Hub”, *J. Coast. Res.*, **2**(65), 1645-1650. <https://doi.org/10.2112/S165-278.1>.
- Ransley, E.J.J., Greaves, D., Raby, A., Simmonds, D. and Hann, M. (2017), “Survivability of wave energy converters using CFD”, *Renew. Energ.*, **109**, 235-247. <https://doi.org/10.1016/j.renene.2017.03.003>.
- Robertson, A., Jonkman, J., Musial, W., Vorpahl, F. and Popko, W. (2013), “Offshore code comparison collaboration, continuation: Phase II results of a floating semisubmersible wind system”, *EWEA Offshore 2013*, November, 1-15.
- Saincher, S. and Banerjee, J. (2016), “Influence of wave breaking on the hydrodynamics of wave energy converters: A review”, *Renew. Sust. Energ. Rev.*, **58**, 704-717. <https://doi.org/10.1016/j.rser.2015.12.301>.
- Schmittner, C.E. (2005), *Rogue Wave Impact on Marine Structures*, Technical University of Berlin.
- Schmittner, C. and Hennig, J. (2012), “Optimization of short-crested deterministic wave sequences via a phase-amplitude iteration scheme”, *Proceedings of the ASME 2012 31st International Conference on Ocean, Offshore and Arctic Engineering*.
- Sirigu, S.A., Bonfanti, M., Begovic, E., Bertorello, C., Dafnakis, P., Giorgi, G., Bracco, G. and Mattiazzo, G. (2020), “Experimental investigation of the mooring system of a wave energy converter in operating and extreme wave conditions”, *J. Mar. Sci. Eng.*, **8**(3). <https://doi.org/10.3390/jmse8030180>.
- Suyuthi, A. and Haver, S.K. (2009), “Extreme loads due to wave breaking Against platform column”, *Proceedings of the 19th (2009) International Offshore and Polar Engineering Conference ISOPE2009*.
- Tampier, G. and Zilic, F. (2018), “Blade-resolved CFD analysis and validation of blockage correction methods for tidal turbines”, (Ed., Guedes Soares), *Advances in Renewable Energies Offshore*, 137-142. Taylor & Francis Group.
- Tampier, G. and Grueter, L. (2017), “Hydrodynamic analysis of a heaving wave energy converter”, *Int. J. Mar. Energ.*, **19**, 304-318. <https://doi.org/10.1016/j.ijome.2017.08.007>.
- Torhaug, R., Winterstein, S.R. and Braathen, A. (1998), “Nonlinear ship loads: Stochastic models for extreme response”, *J. Ship Res.*, **42**(1), 46-55.
- Tromans, P.S., Anaturk, A.R. and Hagemeyer, P. (1991), “A new model for the kinematics of large ocean waves-application as a design wave”, *Proceedings of the 1st International Offshore and Polar Engineering Conference*.
- van Rij, J., Yu, Y.H., Guo, Y. and Coe, R.G. (2019), “A wave energy converter design load case study”, *J. Mar.*

- Sci. Eng.*, 7(8), 1-22. <https://doi.org/10.3390/jmse7080250>.
- Windt, C., Davidson, J. and Ringwood, J.V. (2018), "High-fidelity numerical modelling of ocean wave energy systems: A review of computational fluid dynamics-based numerical wave tanks", *Renew. Sust. Energ. Rev.*, **93**, 610-630. <https://doi.org/10.1016/j.rser.2018.05.020>.
- Yu, Y. and Li, Y. (2011), "Preliminary results of a RANS simulation for a floating point absorber wave energy system in extreme wave conditions", *Omae 2011, 2009*(October), 1-8.

MK